

We are IntechOpen, the world's leading publisher of Open Access books Built by scientists, for scientists

6,900

Open access books available

186,000

International authors and editors

200M

Downloads

Our authors are among the

154

Countries delivered to

TOP 1%

most cited scientists

12.2%

Contributors from top 500 universities



WEB OF SCIENCE™

Selection of our books indexed in the Book Citation Index
in Web of Science™ Core Collection (BKCI)

Interested in publishing with us?
Contact book.department@intechopen.com

Numbers displayed above are based on latest data collected.
For more information visit www.intechopen.com



Outdoor Performance of Perovskite Photovoltaic Technology

Esteban Velilla Hernández, Juan Bernardo Cano Quintero, Juan Felipe Montoya, Iván Mora-Seró and Franklin Jaramillo Isaza

Abstract

In the case of emerging photovoltaic technologies such as perovskite, most published works have focused on laboratory-scale cells, indoor conditions and no international standards have been fully established and adopted. Accordingly, this chapter shows a brief introduction on the standards and evaluation methods for perovskite solar minimodules under natural sunlight conditions. Therefore, we propose evaluating the outdoor performance in terms of power, following the international standard IEC 61853–1 to obtain the performance according to the power rating conditions. After some rigorous experimental evaluations, results shown that the maximum power (P_{\max}) evolution for the analyzed minimodules could be correlated with one of the three patterns commonly described for degradation processes in the literature, named convex, linear, and concave. These patterns were used to estimate the degradation rate and lifetime (T_{80}). Moreover, ideality factor (n_{ID}) was estimated from the open-circuit voltage (V_{oc}) dependence on irradiance and ambient temperature (outdoor data) to provide physical insight into the recombination mechanism dominating the performance during the exposure. In this context, it was observed that the three different degradation patterns identified for P_{\max} can also be identified by n_{ID} . Finally, based on the linear relationship between T_{80} and the time to first reach $n_{\text{ID}} = 2$ ($T_{n_{\text{ID}}=2}$), is demonstrated that n_{ID} analysis could offer important complementary information with important implications for this technology outdoor development, due that the changes in n_{ID} could be correlated with the recombination mechanisms and degradation processes occurring in the device.

Keywords: perovskite solar cell, outdoor performance, solar minimodule, ideality factor, degradation

1. Introduction

Perovskite solar cells (PSCs) have attracted the attention of the scientific community in the last decade evidenced by the impressive number of scientific publications found under the keyword “perovskite & solar cell” in the database SCOPUS¹.

¹ Database SCOPUS, <https://www.scopus.com>, accessed on 24th June of 2021.

At the time of writing, 19407 documents were retrieved, corresponding most of these works to small area devices measured in laboratory conditions. However, for the commercialization of this photovoltaic technology (PV), the main challenge is the fabrication of large area devices with high temporal stability and processed by scalable techniques, being a prerequisite for real-world application reliable measurement of perovskite technology under outdoor conditions. In addition, given the characteristics of metal halide perovskites (denoted as “perovskites” in this work), it is to be noting that there is not a standardized protocol for the fabrication and performance measurements.

The relevance of outdoor performance is supported by a deep analysis of the scientific literature which reveals that only a small fraction of research articles deals with perovskite solar cells measured in outdoor conditions. For instance, only 100 documents were found in SCOPUS when “outdoor” was added as keyword in the search. Thus, less than 1% of the documents reported outdoor measurements, illustrating the wide gap between the development of larger area devices and laboratory scale devices (active area, $A \leq 1 \text{ cm}^2$). Moreover, from the data extracted of more than 16000 scientific articles, almost 70% of these devices have a n-i-p architecture and active area smaller than 1 cm^2 (see **Figure 1a**). This highlighted a big research activity in small devices, contrary to devices with areas closer to commercial applications. In fact, in the case of minimodule (cells connected in series and $A \geq 10 \text{ cm}^2$), there are only 36 devices reported. Interestingly, at this scale the p-i-n architecture account for almost 42% of the devices reported. Thus, this cell configuration is of high interest for scaling up the perovskite technology since it has demonstrated higher stability, reproducibility and can be made from materials of lower cost such Nickel oxide (NiOx) as hole transport layer instead of spiro commonly used for N-I-P devices [1].

On the other hand, related to the reported stability measurements, the T_{80} which is the time at the device achieves 80% of its initial Power Conversion Efficiency (PCE), is plotted against measurement time (**Figure 1b**). Here, the **gray** area in the plot comprises 92.5% of the PSCs which have been tested for periods lower than 1600 hours, far from the temporal stability offered by commercial technologies. A deeper analysis of the data reveals that only 37 devices (~0.09%) have been tested outdoor and only 28 devices have an area larger than 1 cm^2 . The small number of

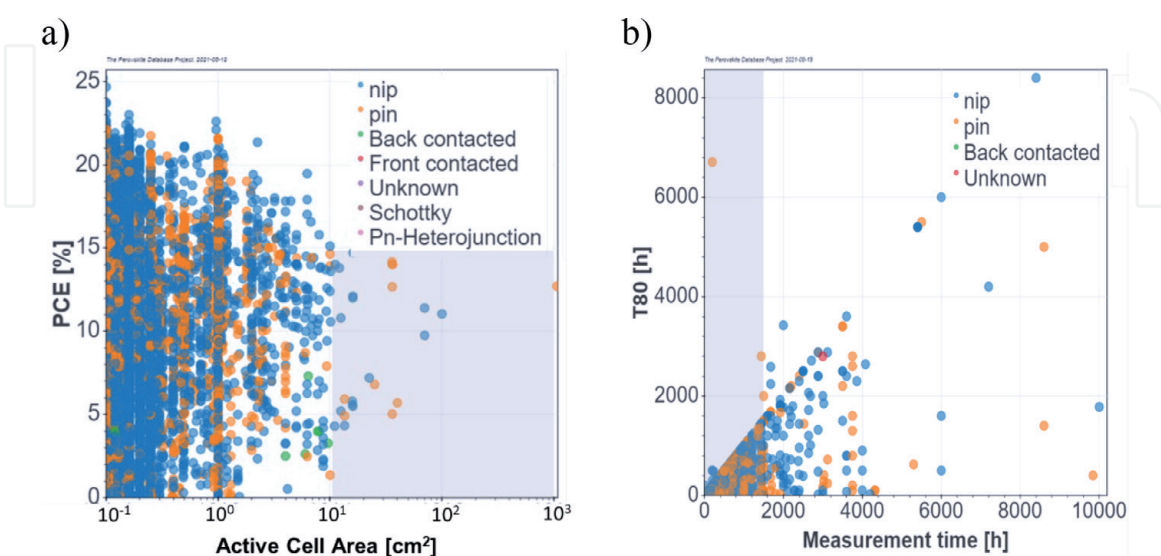


Figure 1. State of the art of perovskite photovoltaic technology. The plots were built using the data available in the “Perovskite Database Project”. (a) PCE as a function of active cell area. The gray area zone corresponds to large area devices ($>10 \text{ cm}^2$). Colors correspond to the cell architecture. (b) T_{80} as a function of measurement time. The gray area corresponds to devices measured for less than 1500 hours. Colors correspond to the cell architecture.

publications dealing with large area PSCs tested under real conditions shows a void in the scientific literature which need to be overcome for commercialization of perovskite technology, considering that the processing techniques and materials used for the fabrication of this PSC are hardly applicable in large area devices, and the last PCE record for PSC of 25.2% is close to commercial technologies such as silicon.

Altogether, this analysis of scientific literature reveals the urgent necessity of studies dealing with performance measurements of large devices operated outdoors, tested for longer periods, and produced by solution-based methods compatible with scalable fabrication. In this chapter, we report a compilation of several studies developed in our group which report the fabrication and electrical performance characterization of perovskite minimodules tested in outdoor conditions for periods as long as 2500 hours. The p-i-n mesoporous structure of the minimodules allows fabrication of devices on substrates of areas up to 100 cm² and showed improved stability and reproducibility of the perovskite films on large-areas [1]. Moreover, the volatile solvent methylamine-acetonitrile used for the perovskite precursor is compatible with scalable fabrication methods [2]. To measure outdoor performance, we propose a methodology based on the international standard IEC 61853-1 [3]. From the temporal evolution of the maximum power (P_{max}) of solar minimodules tracked at the Solar Cell Outdoor Performance Laboratory (OPSUA) of the University of Antioquia, we have collected statistical data which allowed the measurement of lifetime (T_{80}) as well as the temporal evolution of the ideality factor (n_{id}). From these parameters, it is possible to extract the degradation rate and monitor the evolution of the degradation processes. Moreover, the information collected enable tracking the physical processes occurring in the device under real conditions. Finally, the linear relationship between the time at which the module reaches $n_{ID} = 2$ ($T_{n_{ID}2}$) and T_{80} , suggested the complementarity of these two parameters. This complementarity has important implications for improving the characterization and understanding of the degradation processes and, consequently, for the PSC's outdoor optimization.

2. Photovoltaic performance

The performance of photovoltaic devices is conventionally characterized by the I-V curve according to temperature and illumination conditions. Accordingly, the Standard Test Conditions (STC) defined as 1000 W/m² of irradiance and 25°C of cell temperature is the most common conditions to measure the I-V curve in order to extract the main parameters such as open circuit voltage (V_{oc}), short circuit current (I_{sc}), maximum power (P_{max}), and estimate the efficiency [4]. STC is commonly measured in indoor, addressed in the datasheet, and used to compare the progress of solar technologies [5].

Related to outdoor performance, International Electrotechnical Commission (IEC) published a series of standards in IEC 61853 intended to establish the requirements for evaluating the performance of all photovoltaic technologies in term of power [6] or term of energy and performance ratio (IEC 61853-3). In the case of energy, it is worth noting that the study involves the inverter performance. For that, the performance depends on the evaluated solar device, the electronic device, and the maximum power tracking algorithm [7]. In the case of power, the study is mainly based on the parameters extracted for the I-V, in this regard, the standard called "Photovoltaic (PV) module performance testing and energy rating – Part 1: Irradiance and temperature performance measurements and power rating" allows the validation of the devices status of any solar technology defining a pass/fail criteria, in which the success is reached if the power rating conditions (PRC) measured

fall within the power range specified by the manufacturer [6]. Corresponding the conditions for the five power rating conditions to:

- Standard Test Condition (STC), defined at 1000 W/m^2 and cell temperature of 25°C
- Nominal Operating Cell Temperature (NOCT), defined at 800 W/m^2 and ambient temperature of 20°C
- Low Irradiance Condition (LIC), defined at 200 W/m^2 and cell temperature of 25°C
- High Temperature Condition (HTC), defined at 1000 W/m^2 and cell temperature of 75°C
- Low Temperature Condition (LTC), defined at 500 W/m^2 and cell temperature of 15°C

Consequently, the evaluation of the standard IEC61853–1 according to the five PRC provides a complete device characterization under various values of irradiance and temperature, observing the impact of weather variables on P_{max} , V_{oc} , I_{sc} . Besides, this characterization could be carried out using a solar simulator and specialized equipment to set up the temperature and illumination conditions or in natural sunlight with and without a tracker.

In the case of emerging technologies such as PSCs, no international standards have been fully established and adopted, and most published works have focused on laboratory-scale cells to evaluate the performance, stability and degradation of this technology [8–14]. Thus, because this technology is in its infancy, insufficient data are available to fully establish or identify the degradation modes and mechanisms of PSCs, the impact on outdoor performance evolution including large devices [15, 16].

Related to outdoor performance evaluation of perovskite, the International Summit on Organic Photovoltaic Stability (ISOS) suggests 3 protocols [17]. ISOS-O-1 suggests periodically record the J-V curve at STC using a solar simulator (indoor). ISOS-O-2 suggests periodically record the J-V curve under outdoor conditions, keeping the device at the Maximum Power Point (MPP) or open-circuit voltage. In contrast, the ISOS-O-3 suggests periodically recording the J-V curve using a solar simulator, keeping the device at MPP under outdoor conditions. Despite that these cases are related to outdoor, the electrical characterization is usually carried out under indoor conditions to evaluate the performance degradation or device stability, this obviously gives most of the time to over or sub estimate the real device behavior. On the other hand, the protocols suggest reporting the normalized data (per unit) considering the first value to normalize the data and obtain the degradation behavior to estimate degradation rate or lifetime. In this regard, a broadly-supported consensus statement on reporting data related to stability assessment was published, highlighting certain particularities of PSC technology that must be taken into account [14].

3. Outdoor performance

To evaluate the outdoor performance of solar devices under natural sunlight without a tracker, a Solar Cell Outdoor Performance Laboratory of the University of Antioquia (OPSUA, **Figure 2**) was implemented in Medellín-Colombia ($6^\circ 15' 38''$

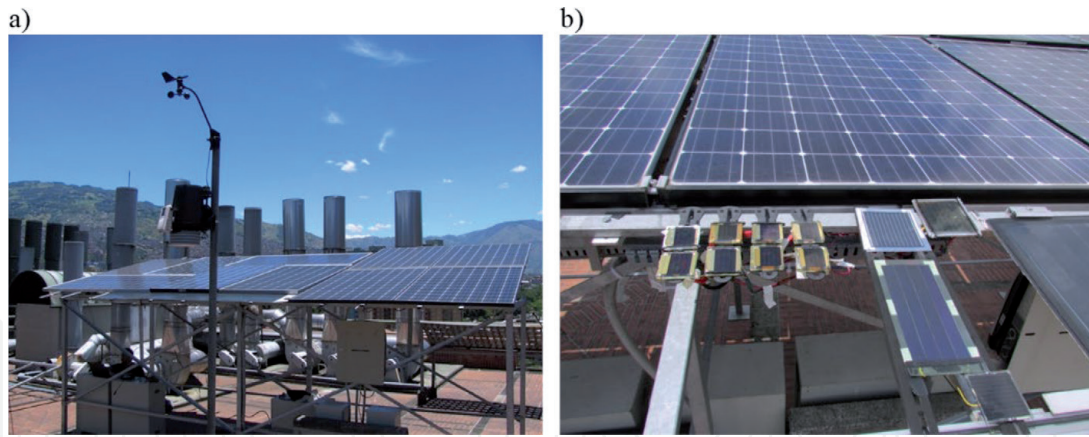


Figure 2. Solar Cell Outdoor Performance Laboratory of the University of Antioquia (OPSUA). a) commercial technologies. b) perovskite devices.

N 75° 34' 05''W, facing south at a fixed angle of 10°). In this laboratory, the performance of photovoltaic technologies could be evaluated in terms of power measuring the I-V curve of devices under different illumination and temperature conditions according to IEC 61853-1.

To measure the I-V curve of solar devices different hardware techniques have been used [18], intended to improve portability, local data storage, low cost, and faster response during measurement. Two different types of I-V curve tracers (solar analyzer, SA) have been recently developed [19]. One SA is based on the capacitive load technique due to simplicity, power dissipation, and cost concerns. This prototype is intended for devices that operate for voltages up to 250 V and currents up to 12.5 A (solar panels, **Figure 3a**), measuring the I-V curve from short circuit to open circuit. The other SA is based on the four-quadrant DC supply due to greater flexibility on sweep direction and speed, allowing a complete characterization including the reverse bias region and voltages higher than the open-circuit voltage, making it practical for hysteresis measurements. This prototype is intended for devices that operate for voltages up to 8 V and currents up to 3 A (solar cells and solar minimodules, **Figure 3b**). Moreover, to optimize the I-V curve process and store records, an embedded computer (Raspberry Pi) is connected to control each SA and measure the I-V curve every minute.

3.1 Methodology to estimate the performance from outdoor tests

The monitoring system implemented in OPSUA, allows to record, and store the weather variables (irradiance and temperatures), and electrical data (I-V curve). These data are uploaded to the remote server to provide backup, and centralize the

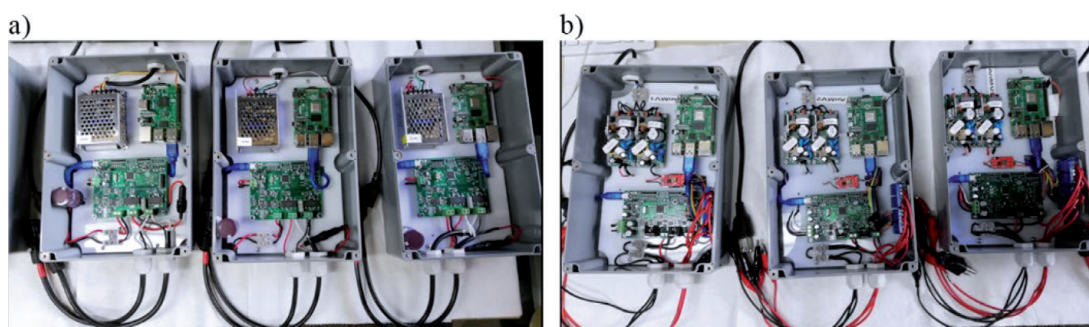


Figure 3. Solar analyzers (SA) to tracer the I-V curve. a) SA for solar panels and b) SA for solar cells or minimodules.

process to estimate the Outdoor performance according to the flowchart shows in **Figure 2** considering the power rating conditions suggested by IEC 61853–1. In this sense, the implemented procedure to estimate the outdoor performance could be divided into two main parts: one part is related to the databases of exposed devices that are created by merging the weather and electrical data, another part is related to the analysis, **Figure 4**.

In brief, from the I-V curves, photovoltaic parameters such as V_{oc} , the short-circuit current (I_{sc}), the fill factor (FF), the photoconversion efficiency, and P_{max} were extracted. The irradiances and ambient temperatures were also recorded during the I-V measurement (synchronously). Subsequently, the raw data are filtered based on the linearity determination criterion to minimize transient effects related to changes in irradiance, shadowing caused by clouds or droplets, or atypical data [20]. Hence, the best-fit data with a deviation of $\pm 5\%$ were selected as the filtered data. These filtered data are used to perform the analyses:

- Outdoor performance (OP): the impact of weather variables on performance is estimated and depicted in form of map to illustrate the performance as a function of irradiance and temperature, representing the average outdoor performance during the evaluated time and indicating the operative range of the involved variables (**Figure 5a**). A full description of these maps was shown in previous work [19–21].
- Power rating conditions (PRCs): the data shown in the form of maps (the average OP) are filtered considering a deviation of 5% from the irradiance levels corresponding to the power rating conditions indicated by IEC 61853–1, that is, 1000 W/m^2 , corresponding to standard test conditions (STC); 800 W/m^2 , corresponding to NOCT conditions; 500 W/m^2 , corresponding to low-temperature conditions (LTC); and 200 W/m^2 , corresponding to low-irradiance conditions (LIC). Hence, the data deviation of each power rating conditions is considered by the median value of the data considered in each sampling time, **Figure 5b**.

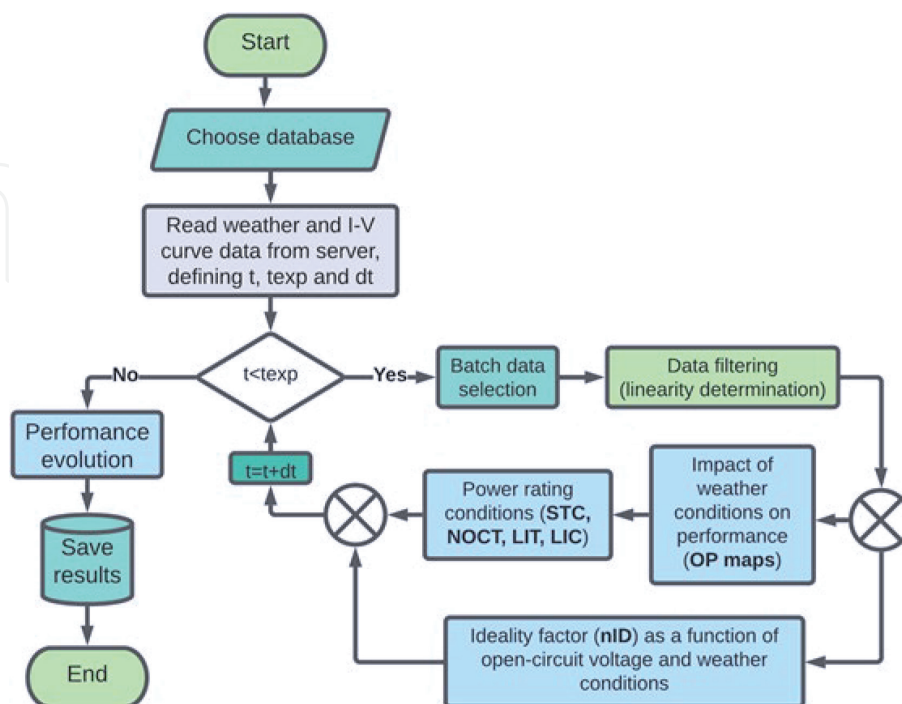


Figure 4.

Flow chart to obtain the outdoor performance. Procedure to analyze and process the databases to obtain the impact of weather variables on outdoor performance (OP), power rating conditions (PRCs), and ideality factor (nID).

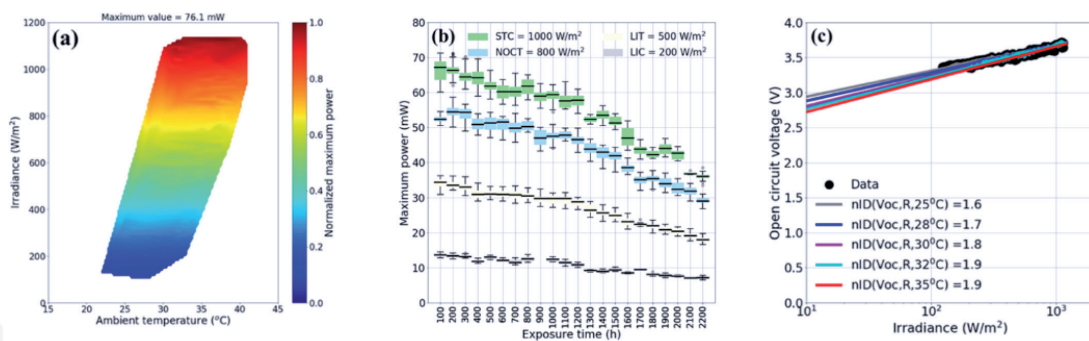


Figure 5. Outdoor analysis. a) Outdoor performance displayed in the form of a map to show the impact of weather variables on performance. b) Calculated PRCs over time by filtering the data by batches considering the irradiance levels defined by the power rating conditions. c) Ideality factor estimated considering the ambient temperature and the data shown in figure a).

c. Ideality factor (n_{ID}): n_{ID} is calculated following the procedure shown [21], considering the filtered data and processing the data at different ambient temperatures between 25 and 35°C (Figure 5c). Consequently, because different ideality factors can be calculated, the median value is considered the average value to consider the data dispersion representing the evaluated time window.

Finally, it is worth noting that these analyses are considered by the loop. For that, it is possible to divide the data by sets (batches) to estimate the average impact of weather variables on performance, the power rating conditions and ideality factor in every dataset (batch). Therefore, it is possible to analyze the performance evolution or power loss tendency (degradation-shape).

3.2 Perovskite outdoor performance

In OPSUA, perovskite minimodules (PMM) with inverted structure, large areas and different cells in series have been tested [1, 20, 21]. Figure 6 shows the performance for three representative PMMs during the first 100 h of exposure in the form of contour. These maps represent the average performance allowing observation of the impact of weather variables on P_{max} , V_{oc} , and I_{sc} . In this cases is noting that the performance for the samples show in Figure 6a, b, d, e, g and h, follow similar and expected behavior for P_{max} , I_{sc} , and V_{oc} according to the irradiance. However, the performance shows in Figure 6c, f and i do not exhibit this monotonic behavior, showing local maxima or minima at various irradiance levels and temperature, behavior that was correlated with fast degradation processes during the first 100 h of exposure [21]. Therefore, these maps could be used as a diagnostic tool aimed at identifying early faults or degradation processes in the devices. Moreover, the maps allow us to identify the low-temperature dependence of V_{oc} , which was identified as a competitive advantage of perovskite [20].

3.3 Perovskite degradation

Information on system state and performance collected over time is referred to as degradation data [22]. In solar devices (cells, modules, and panels), the natural indicator to evaluate the degradation is the performance, which is commonly obtained from the I-V curves data and contrasted to weather variables such as irradiance and temperature [23]. In this sense, the failure for an individual device could be defined as the time at which the output power dropped to 20% below the initial output, being this the standard definition of lifetime of photovoltaic devices (T_{80}). It depends on

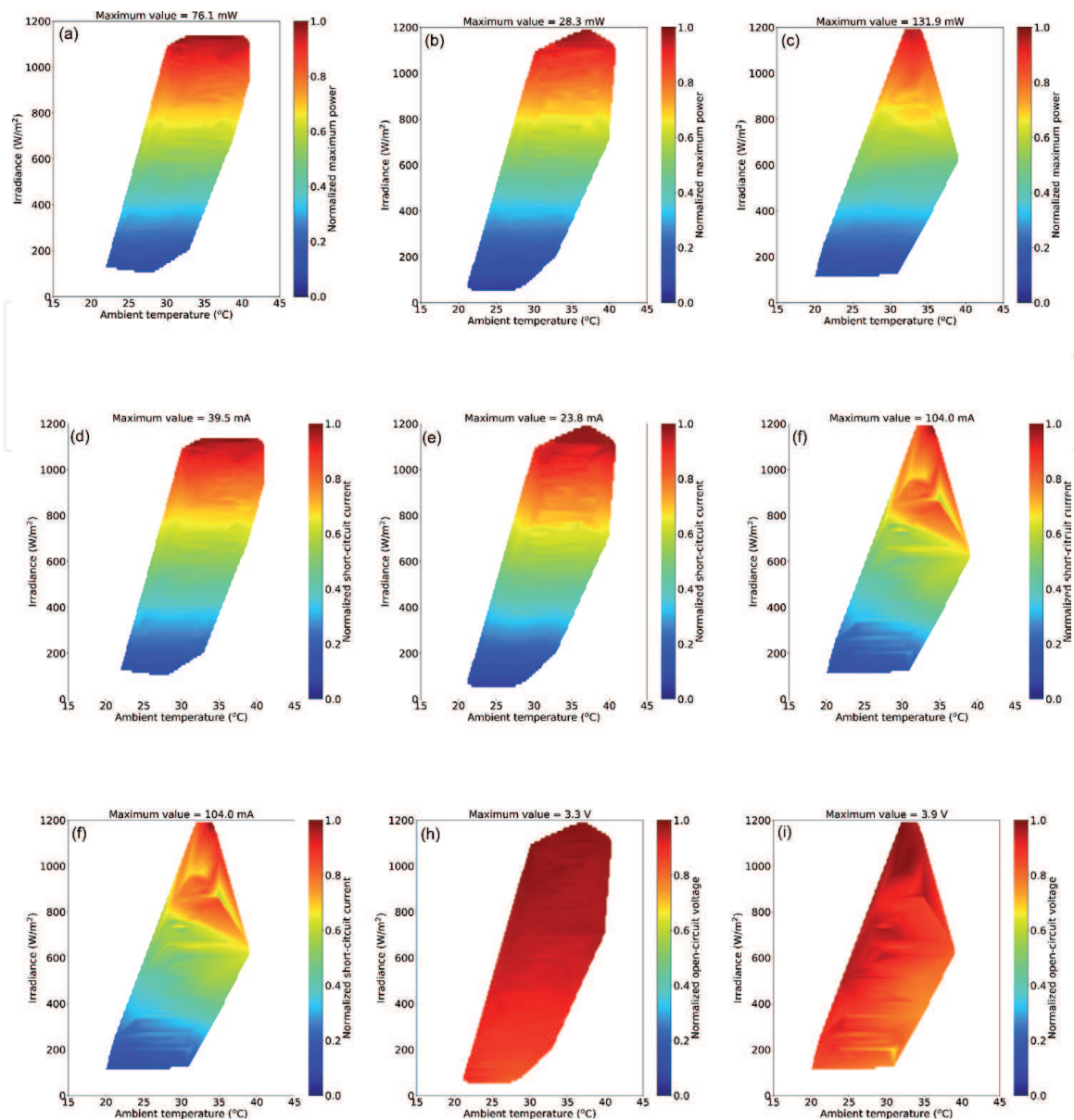


Figure 6.

Normalized outdoor performance of three representative PMM. a-c) Maximum power. d-f) Short-circuit current. g-i) Open-circuit voltage. The color bar indicates the variable range. At the top of each plot, the maximum recorded value used to normalize each variable's data is shown. These figures only considered the data during the first 100 h of exposure. Figure taken from [21]. Copyright 2021, Springer Nature.

different factors such as materials and procedures used in the device fabrication, cell interconnects, weather conditions, seasonal variations, installation conditions, shading and soiling effects, an electrical mismatch between cells, among others [24].

Currently, the long-term stability or lifetime (T_{80}) of perovskite technology on average is only a few months, even for encapsulated devices, corresponding to a degradation rate higher than 100%/year [25]. This short lifetime is the result of intrinsic and external aspects [26]. The intrinsic degradation is mainly related to thermal and light soaking effects, while external degradation is mainly related to the ingress of water, moisture, or oxygen into the device [27, 28]. Accordingly, it is possible to find different strategies to improve the lifetime, including the encapsulation process/method, kind of perovskite (2D, 3D, Etc.), selective charge contacts or other layers involved [29], passivation of the interfaces [30] or the grain boundaries [31]. Nevertheless, because the degradation is a complex process that depends on the structure (layers) and their interfaces, the degradation studies must be conducted in the complete device and not in isolated layers [32].

In this regard, **Figure 7** shows a summary of P_{\max} evolution for different minimodules evaluated under outdoor conditions in OPSUA. Here, to show the performance degradation, the evolution of the performance at NOCT was selected because this power rating conditions is defined as the equilibrium mean solar cell junction temperature of the module in the described environment [33], these conditions reflecting adequately the real operating, indicating how the module temperature is affected by solar irradiation, ambient temperature and thermal properties of the photovoltaic material [34]. In addition, these conditions are included on the datasheets for commercial solar modules, and it can be reached outdoors [19] while the STC conditions rarely occur outdoor [35].

The evaluated outdoor samples exhibited three different P_{\max} evolution patterns over time, named convex, linear, and concave patterns, because of the shapes they exhibit. These three distinctive patterns are commonly described for degradation processes in the literature to study possible degradation paths and estimate the failure time [22]. Therefore, these P_{\max} behaviors were fitting to linear models to estimate the degradation rate and T_{80} . Thus, the T_{80} values for the samples were analyzed in **Figure 7b** in the form of probability distribution plot. This plot indicates that the double Weibull distribution is more suitable to represent the data distribution with a shape parameter of $c = 0.6$, suggesting higher early mortality of devices and that the failure rate decreases over time. Also, this result suggested 3 degradation levels based on the likelihood of T_{80} values. The first was related to the most likely and faster degradation ($T_{80} < 200$ h), the second related to moderate degradation ($350 < T_{80} < 700$ h), and the third related to lower degradation ($T_{80} > 1250$ h). These levels or groups agree with the degradation shape of concave, linear, and convex patterns, respectively. Therefore, all the analyzed minimodules present behavior that can be statistically associated with these three patterns. Finally, **Figure 7c** highlights the behavior of one representative sample of each pattern, corresponding to the lower degradation rate of the initial P_{\max} of 0.29%/day to the convex pattern, a moderate degradation rate of 1.39%/day to the linear pattern, and faster degradation rate of 7.68%/day to the concave pattern.

It is worth noting that these three P_{\max} patterns have all been observed for PSCs [25]. For instance, the convex pattern has been observed for encapsulated PSCs stored at room temperature [36]. The linear and convex patterns have been observed in nonencapsulated cells under controlled relative humidity conditions [37],

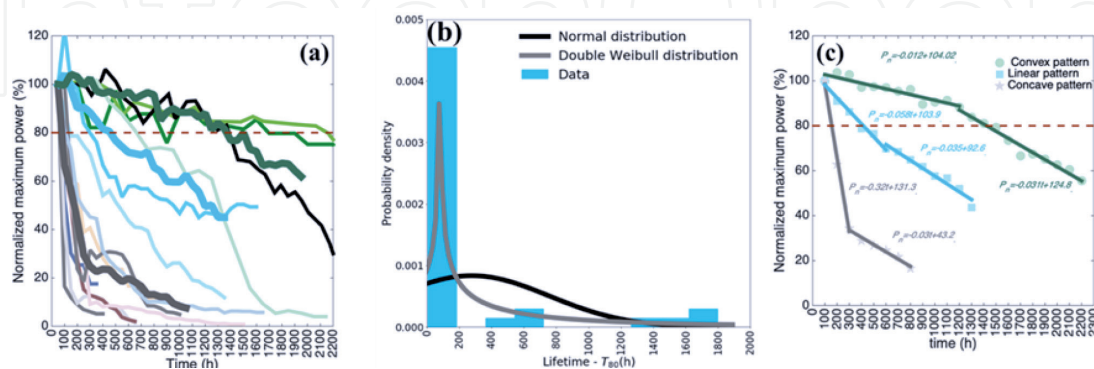


Figure 7. Summary of P_{\max} evolution at NOCT from the outdoor test. a) representative power loss tendencies for perovskite minimodules. b) Probability density of T_{80} for evaluated samples. Corresponding the blue bars to T_{80} data, black line to data fit to Normal Distribution function (being the parameters: $\mu = 276.8$ and $std. = 478$) and green line to data fit to Double Weibull Distribution function (being the parameters: $c = 0.6$, $loc = 80$ and $scale = 453.7$). c) Degradation Rate (DR) of three representative patterns of each group according to degradation levels suggested by the probability function distribution of T_{80} . Corresponding the DR to the slope of linear fitting showed (color lines). The slope of the fitted curves provides the degradation rate in %/h units.

while the concave pattern has been observed in encapsulated cells exposed to different levels of sunlight [9]. In addition, this shape has also been observed in nonencapsulated PSCs under higher relative humidity [11], and in nonencapsulated devices tested under air exposure [38]. Nevertheless, in the case of controlled atmospheres is possible to correlate the performance behavior with the physical origins of the degradation, whereas under outdoor conditions is not easy to determine the origin of the degradation.

In the case of the representative samples of each P_{\max} pattern obtained from the outdoor tests (**Figure 7**), The degradation in P_{\max} can be mainly attributed to the decreases in V_{oc} or I_{sc} for the convex and linear patterns, respectively (**Figure 8a and b**). In contrast, both parameters are significantly degraded for the concave pattern, as is shown in **Figure 8c**. Fitting the normalized variables concerning the initial values, to linear regression models in order to estimate the degradation rates (DR) by sections (**Figure 8d–f**), is possible to observe some features:

- Related to P_{\max} convex pattern, this variable, and the V_{oc} can be modeled by 2 linear models, corresponding the DR value for the second section to 2 times first section's value for both variables. In contrast, the I_{sc} can be modeled by only one linear model characterized by a DR value of 0.0023%/h. These results indicated that the main power drop is because of the changes in V_{oc} .
- Related to P_{\max} linear pattern, this variable, and the V_{oc} can be modeled by 2 linear models. Nevertheless, the corresponding DR value for the second section for P_{\max} is lower than the DR value of the first section (0.035 and 0.058%/h, respectively). For V_{oc} , the DR for the second section is

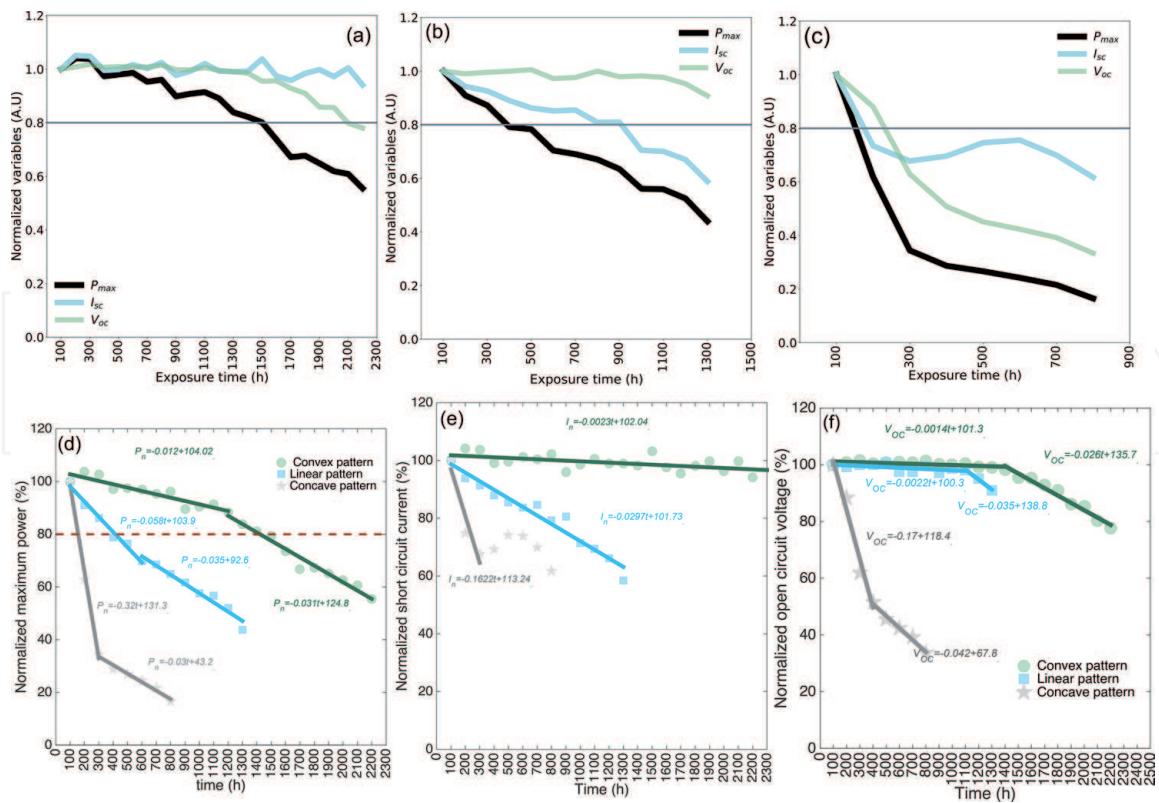


Figure 8.

Normalized behavior for photovoltaic parameters. Corresponding a) for variables related to P_{\max} convex pattern, b) for P_{\max} linear pattern, and c) for P_{\max} concave pattern. d) Maximum power for all patterns. e) I_{sc} for all patterns and f) V_{oc} for all patterns. The green color corresponds to P_{\max} convex pattern, the blue color corresponds to P_{\max} linear pattern, and the gray color corresponds to P_{\max} concave pattern. Solid lines correspond to the fits and color markets to the data.

16 times the first section's value (0.035 and 0.0022%/h, respectively). I_{sc} can be modeled by only one linear model characterized by a DR value of 0.0029%/h. These results indicated that the main power drop is because of the changes in I_{sc} .

- c. Related to P_{max} concave pattern, all variables can be modeled by 2 linear models, corresponding the second section's DR values to the lower DR values for each variable. Moreover, in the first section, similar DR values for V_{oc} and I_{sc} were obtained. These results indicated that the power drop is because of both variables' changes (I_{sc} and V_{oc}).
- d. Accordingly, P_{max} convex and linear patterns share similar trends, characterized by constant DR for I_{sc} , indicating a constant reduction in the charge extraction. Also, both V_{oc} patterns shown a double increase in the DR after a specific time (1400 and 1000 h for convex and linear patterns). This fact could be associated with surface traps allowing the charge recombination, increasing the device's series resistance, and causing the voltage drop.

3.4 Ideality factor (n_{ID})

The ideality factor also called the quality factor or shape curve factor, is one of the most reported parameters for different solar cell technologies. This parameter has been used to define the electrical behavior of solar devices due to its relationship with conduction, transport, recombination, and behavior at interface junctions, providing direct information on the dominating recombination processes. For silicon, n_{ID} has been widely studied, reporting values between 1 and 2. Close to 1 indicates ideal junctions, equal to 2 is correlated with the degradation of the solar cell, non-uniformities on recombination centers, and shunt resistance effects [39]. This parameter has been estimated using the relationship between the open-circuit voltage (V_{oc}) and light intensity to overcome the effects of series resistance [40], performing numerical calculations [41], and fitting the I-V curves to equivalent circuits [42]. In the case of perovskite, a full interpretation of n_{ID} for non-encapsulated cells was reported, establishing the relationship between the dominating recombination process, light intensity and V_{oc} [43]. In addition, under dark conditions, ideality factors close to 2 have been reported due to carrier recombination and trap-assisted recombination [44, 45] and values between 1.3 and 2.5 has been estimated considering several hole transport layer thicknesses [46]. Moreover, due to the estimation of this parameter could be affected by different aspects such as hysteresis, the dependence of open-circuit voltage on light intensity and temperature, parasitic resistances, among others, the perovskite ideality factor estimated from the dark I-V curve could be higher than 2 [47]. Nevertheless, an agreement has been shown between the n_{ID} value estimated from the recombination resistance extracted through impedance/frequency-response (IFR) analysis and the value calculated from V_{oc} at different light intensities [21, 47, 48].

On the other hand, despite that n_{ID} can be accurately estimated from the I-V curve using proper optimization methods [49], this procedure could be considered as successful if the I-V curves are well defined. In cases in which the I-V curves show an S-shape, this procedure could not be suitable, and other elements in the equivalent circuit such as another diode have been included to reproduce the I-V behavior, increasing the complexity and accurate interpretation of ideality factor [42, 50]. The S-shape behavior is associated with the chemical degradation of electrical

contacts or charge accumulation on electrodes affecting the series resistance of the device [51]. Thus, to avoid the series resistances issues, another method is used to estimate the n_{ID} the relationship between V_{oc} and light intensities, Eq. (1). This equation shows the relationship between the V_{oc} , bandgap (E_g), thermal voltage, ideality factor, and logarithmic dependence on light.

$$e \cdot V_{oc} = m \cdot E_g + n_{ID} \cdot k_B \cdot T \cdot m \cdot \ln \frac{G}{G_0} \quad (1)$$

Where e is the electron charge, m is the number of equal cells connected in series, E_g is the light absorber bandgap, k_B is the Boltzmann constant, T is the temperature, G is the irradiance or light intensity, and G_0 is a constant with the same units than G .

Accordingly, the outdoor data related to the three representative samples correlated to each P_{max} pattern were analyzed following Eq. (1). Therefore, the average n_{ID} values were calculated from the outdoor data taking advantage of the different levels of illumination caused by day-night cycles to collect a large amount of data across a broad range of illumination conditions.

Figure 9 shows as an example the procedure to estimate the n_{ID} using the outdoor data for the sample with P_{max} convex pattern during the first 100 h of exposure. The raw data (full data during the first 100 h) are filtered, applying a linearity determination criterion to minimize the influence of atypical data or data related to unclear days, shadowing, dirt, or droplets on the surface. In this regard, the best-fit data with a deviation of $\pm 5\%$ are selected as the filtered data, representing the average conditions during the exposure time, **Figure 9a**. Then, the data are filtered by the ambient temperature to extract the V_{oc} and irradiance values correlated to this temperature. These V_{oc} and irradiance values are used in accordance with Eq. (1) to estimate the n_{ID} values, **Figure 9b**. Accordingly, to consider the deviations from the average value due to temperature changes, n_{ID} values are estimated by calculating this parameter in the measurement sets, filtering the data by temperatures between 25 and 37°C in steps of 2°C with a deviation of $\pm 1^\circ\text{C}$.

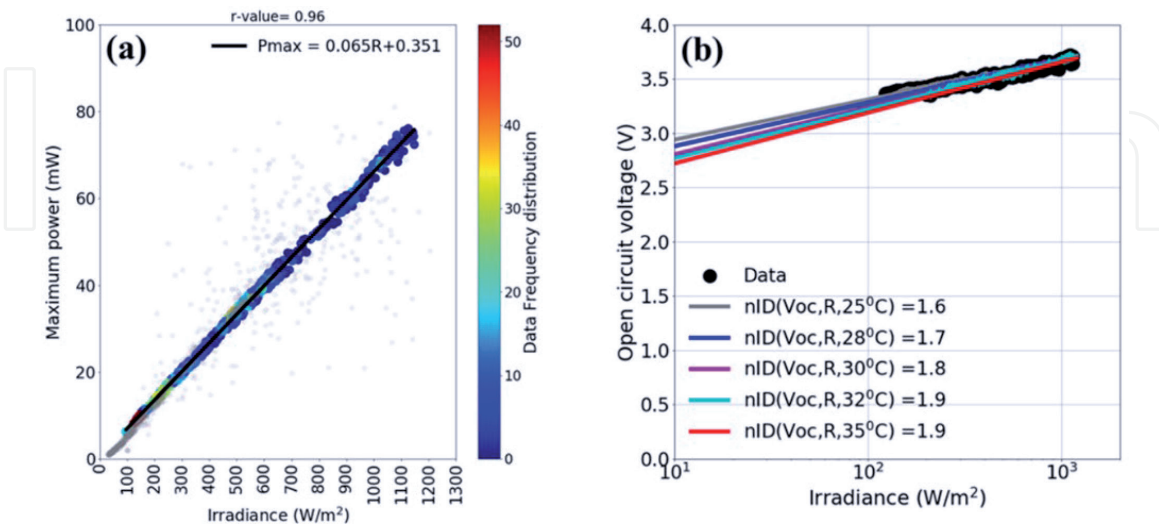


Figure 9.

*Procedure to estimate n_{ID} from Outdoor Data. a) Linearity determination criteria to filter the data from atypical data. At the top is shown the coefficient of determination (r -value), estimated from the fitting process between P_{max} and irradiance. The gray points correspond to data measured in the considered exposure time, and the color dots correspond to data considered as filtered and representative of the dataset. The filtered data correspond to the average conditions during the 100 h of exposure. b) Ideality factor estimated considering different ambient temperatures and the data registered between 0 and 100 h of exposure. The parameters estimation of n_{ID} for the linear regression in accordance with Eq. (1) is shown in **Table 1**.*

Temperature (°C)	n_{ID}	r-value	Slope	Intercept
25	1.58	0.98	0.16	2.57
28	1.67	0.98	0.17	2.48
30	1.81	0.99	0.18	2.37
32	1.86	0.99	0.19	2.32
35	1.91	0.97	0.20	2.25

Table 1.
 Parameters related to the fit of V_{oc} and Irradiance to estimate n_{ID} .

Then the mean value of each dataset is considered as the average n_{ID} value. The results during the exposure time for the representative samples are shown in **Figure 10** in the form of boxplots to illustrate the deviations from the average value and data distribution for the samples analyzed.

The n_{ID} results showed in **Figure 10** also exhibits three distinct evolution patterns or shapes. Precisely, a convex P_{max} evolution pattern corresponds to a concave n_{ID} evolution pattern (**Figure 10a**) and *vice versa* (**Figure 10c**). In contrast, for a linear P_{max} pattern, a linear n_{ID} pattern is observed (**Figure 10b**). In the cases of convex P_{max} /concave n_{ID} patterns (**Figures 9 and 10a**) and linear patterns (**Figures 9 and 10b**), at times earlier than T_{80} (1442.2 and 414.2 h, respectively), n_{ID} takes values between 1 and 2, indicating bulk Shockley-Read-Hall (SRH) recombination [43]. For longer times, n_{ID} exhibits values above 2, characteristic of a multiple-trap distribution, originating from the formation of trap states, causing the performance degradation, as pointed out by Khadka et al. [36]. In concave P_{max} /convex n_{ID} patterns (**Figures 9 and 11c**), the initial values of n_{ID} are higher than 2, indicating fast degradation in the first 100 h of exposure due to the formation of multiple trap states. Interestingly, after the initial increase in n_{ID} , a progressive decrease is observed in the concave and convex (**Figure 11a and c**) cases, suggesting evolution from bulk recombination to interfacial recombination. This behavior does not imply a recovery in device performance; it only indicates a transition between two different recombination regimes in the degradation process, from multiple-trap recombination to a regime with higher interfacial recombination.

It is worth noting that results in **Figure 10** were estimated in accordance with Eq. (1) using the ambient temperature to simplify the methodology and the number of variables to record in the outdoor test. Nevertheless, to determine the impact of

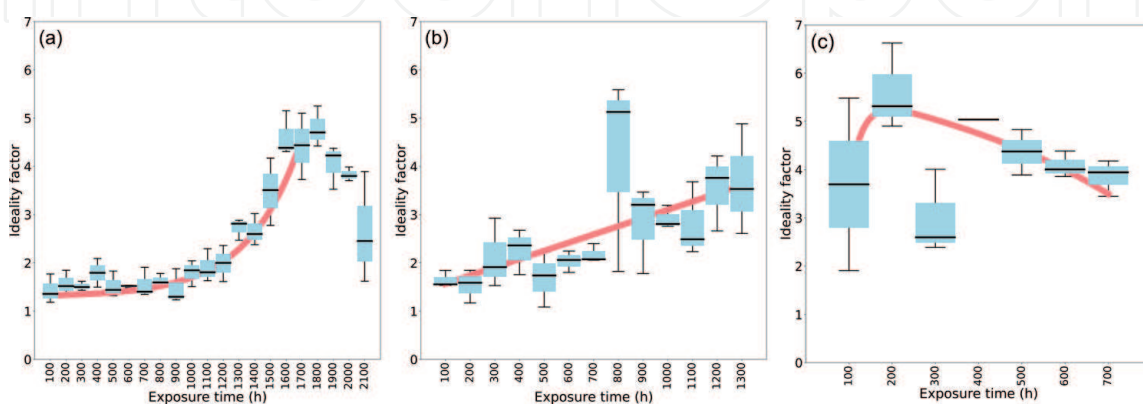


Figure 10.
 Patterns of the ideality factor. a-c) Ideality factor analysis of the three representative samples: (a) n_{ID} exhibits a concave pattern, (b) n_{ID} exhibits a linear pattern, and (c) n_{ID} exhibits a convex pattern. The thick black line on each box represents the average value in the corresponding time window. The red line is included as a visual guide to illustrate the patterns. Figure taken from [21]. Copyright 2021, Springer Nature.

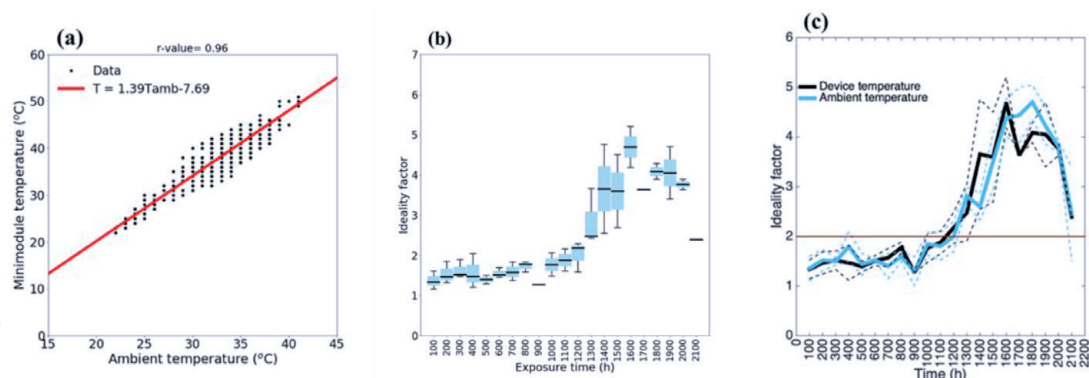


Figure 11.

Estimated ideality factor using the device temperature. a) Relationship between ambient and minimodule temperature during the first 100 h of exposure. Corresponding the points to measured data and the solid red line to the linear regression fit. The corresponding coefficient of determination of the fits is shown at the top. b) Ideality factor calculated considering the device temperature instead of the ambient temperature. The boxplots were obtained by calculating the variables observed in the measurement sets, each of which contained measurements recorded over 100 hours of outdoor exposure. The thick black line on each box represents the median value, while the blue boxes represent 50% of the data in the corresponding time window. c) Comparison of ideality factor calculated using the device and ambient temperature. Solid lines of each color correspond to the estimated average n_{ID} values and dotted lines to the standard deviation of the variables. These values were estimated by calculating the n_{ID} values in the corresponding time window for ambient temperatures ranging between 25 and 35°C and device temperature between 25 and 45°C in steps of 2°C.

the device temperature in the estimation of the ideality factor, the data related to P_{max} convex pattern were used to estimate this parameter. In this sense, **Figure 11a** shows the relationship between ambient and device temperature, which depicted a linear behavior characterized by the figure's inset equation and demonstrated by the r -value close to 1 shown at the top. **Figure 11b** shows the results of calculating the n_{ID} using the device temperature. This behavior is very similar to the n_{ID} behavior obtained in **Figure 10a** using the ambient temperature. Therefore, to compare in a better way both behaviors, **Figure 11c** shows the average values and standard deviation of the variable in the measurements sets, which contain the data over 100 h of exposure. Hence, the error between both estimations was 4.3%, which was calculated using the Euclidean norm between the difference of both estimations. Consequently, it was possible to validate that using the ambient temperature instead of device temperature allowed us to estimate reliable values to track the evolution (because this estimation introduces a relative error lower than 5%) and simplifies the number of outdoor variables.

4. Conclusions

Outdoor performance of emerging halide perovskite photovoltaics is just starting to become an important issue to determine the technology behavior under more realistic conditions. Specific standards are required to be applied for particular technologies specially for halide perovskite solar devices, as their behavior not necessarily follows the typical silicon or other traditional semiconductors based technology. However, general standards like IEC 61853–1 allows to establish valid criteria to study these emerging devices. Parameters as lifetime (T_{80}) and ideality factor (n_{ID}) can be estimated from the maximum power output trends and open-circuit voltage (V_{oc}) dependence on irradiance and ambient temperature from outdoor data. Moreover, the values can provide physical insight into the recombination mechanism dominating the performance during the exposure. Perovskites degradation indicates both bulk Shockley-Read-Hall (SRH) recombination and multiple-trap states for higher values of ideality factor. These methodologies allow to continue studying different architectures,

composition, encapsulating methods to improve the performance of the perovskite photovoltaics under outdoor conditions before they can be release into market.

Acknowledgements

The authors gratefully acknowledge the financial support provided by the Colombia Scientific Program within the framework of the call *Ecosistema Científico* (contract no. FP44842—218-2018). Esteban Velilla thanks to the Ministry of Science, Technology and Innovation (Minciencias) for national doctoral scholarship number 727–2015 (contract no. FP44842–124-2017). Iván Mora-Seró thanks the European Research Council (ERC) funding for this work via a Consolidator grant (no. 724424—No-LIMIT).

Conflict of interest

The authors declare no conflict of interest

Author details

Esteban Velilla Hernández^{1,2*}, Juan Bernardo Cano Quintero¹, Juan Felipe Montoya², Iván Mora-Seró³ and Franklin Jaramillo Isaza²

1 Grupo en Manejo Eficiente de la Energía (GIMEL), Universidad de Antioquia, UdeA, Medellín, Colombia

2 Centro de Investigación, Innovación y Desarrollo de Materiales (CIDEMAT), Universidad de Antioquia, UdeA, Medellín, Colombia

3 Institute of Advanced Materials (INAM), Jaume I University, Castelló de la Plana, Spain

*Address all correspondence to: esteban.velilla@udea.edu.co

IntechOpen

© 2021 The Author(s). Licensee IntechOpen. This chapter is distributed under the terms of the Creative Commons Attribution License (<http://creativecommons.org/licenses/by/3.0>), which permits unrestricted use, distribution, and reproduction in any medium, provided the original work is properly cited. 

References

- [1] Ramirez D, Velilla E, Montoya JF, Jaramillo F. Mitigating scalability issues of perovskite photovoltaic technology through a p-i-n meso-superstructured solar cell architecture. *Sol Energy Mater Sol Cells* [Internet]. Elsevier B.V.; 2019;195:191-7. Available from: <https://linkinghub.elsevier.com/retrieve/pii/S0927024819301217>
- [2] Wu C, Wang K, Li J, Liang Z, Li J, Li W, et al. Volatile solution: the way toward scalable fabrication of perovskite solar cells? *Matter* [Internet]. Elsevier Inc.; 2021;4:775-93. Available from: <https://doi.org/10.1016/j.matt.2020.12.025>
- [3] Velilla Hernandez E. Computational Modeling of the Electrical Performance and Degradation of Third-generation Photovoltaic Modules, Under Accelerated and Real Operating Conditions [Thesis] [Internet]. Antioquia University; 2021. Available from: <http://hdl.handle.net/10495/20696>
- [4] IEC 61215-1-2. Terrestrial photovoltaic (PV) modules – Design qualification and type approval – Part 1-2: Special requirements for testing of thin-film Cadmium Telluride (CdTe) based photovoltaic (PV) modules. 2004.
- [5] Green M, Dunlop E, Hohl-Ebinger J, Yoshita M, Kopidakis N, Hao X. Solar cell efficiency tables (version 57). *Prog Photovoltaics Res Appl* [Internet]. John Wiley and Sons Ltd.; 2021;29:3-15. Available from: <https://onlinelibrary.wiley.com/doi/10.1002/pip.3371>
- [6] IEC 61853-1. Photovoltaic (PV) module performance testing and energy rating - Part 1: Irradiance and temperature performance measurements and power rating. *Int. Electrotech. Comm.* 2011.
- [7] Eltamaly AM, Farh HMH, Othman MF. A novel evaluation index for the photovoltaic maximum power point tracker techniques. *Sol Energy* [Internet]. Elsevier; 2018;174:940-56. Available from: <https://doi.org/10.1016/j.solener.2018.09.060>
- [8] Holzhey P, Saliba M. A full overview of international standards assessing the long-term stability of perovskite solar cells. *J Mater Chem A* [Internet]. 2018;6:21794-808. Available from: <http://pubs.rsc.org/en/Content/ArticleLanding/2018/TA/C8TA06950F>
- [9] Anoop KM, Khenkin M V., Di Giacomo F, Galagan Y, Rahmany S, Etgar L, et al. Bias-Dependent Stability of Perovskite Solar Cells Studied Using Natural and Concentrated Sunlight. *Sol RRL* [Internet]. Wiley; 2020;4:1900335. Available from: <https://onlinelibrary.wiley.com/doi/abs/10.1002/solr.201900335>
- [10] Yang J, Siempelkamp BD, Liu D, Kelly TL. Investigation of CH₃NH₃PbI₃ Degradation Rates and Mechanisms in Controlled Humidity Environments Using in Situ Techniques. *ACS Nano* [Internet]. 2015;9:1955-1963. Available from: <http://pubs.acs.org/doi/10.1021/nn506864k>
- [11] Domanski K, Alharbi EA, Hagfeldt A, Grätzel M, Tress W. Systematic investigation of the impact of operation conditions on the degradation behavior of perovskite solar cells. *Nat Energy* [Internet]. 2018;3:61-67. Available from: <http://www.nature.com/articles/s41560-017-0060-5>
- [12] Cheacharoen R, Rolston N, Harwood D, Bush KA, Dauskardt RH, McGehee MD. Design and understanding of encapsulated perovskite solar cells to withstand temperature cycling. *Energy Environ Sci* [Internet]. Royal Society of Chemistry; 2018;11:144-150. Available from: <http://dx.doi.org/10.1039/C7EE02564E>

- [13] Tress W, Domanski K, Carlsen B, Agarwalla A, Alharbi EA, Graetzel M, et al. Performance of perovskite solar cells under simulated temperature-illumination real-world operating conditions. *Nat Energy* [Internet]. 2019;4:568-74. Available from: <http://www.nature.com/articles/s41560-019-0400-8>
- [14] Khenkin M V., Katz EA, Abate A, Bardizza G, Berry JJ, Brabec C, et al. Consensus statement for stability assessment and reporting for perovskite photovoltaics based on ISOS procedures. *Nat Energy* [Internet]. 2020;5:35-49. Available from: <http://www.nature.com/articles/s41560-019-0529-5>
- [15] Hu Y, Chu Y, Wang Q, Zhang Z, Ming Y, Mei A, et al. Standardizing Perovskite Solar Modules beyond Cells [Internet]. *Joule*. 2019. p. 2076-2085. Available from: <https://linkinghub.elsevier.com/retrieve/pii/S2542435119304180>
- [16] Qiu L, He S, Ono LK, Liu S, Qi Y. Scalable Fabrication of Metal Halide Perovskite Solar Cells and Modules [Internet]. *ACS Energy Lett*. 2019. p. 2147-67. Available from: <http://pubs.acs.org/doi/10.1021/acsenerylett.9b01396>
- [17] Reese MO, Gevorgyan SA, Jørgensen M, Bundgaard E, Kurtz SR, Ginley DS, et al. Consensus stability testing protocols for organic photovoltaic materials and devices. *Sol Energy Mater Sol Cells* [Internet]. Elsevier B.V.; 2011;95:1253-67. Available from: <https://linkinghub.elsevier.com/retrieve/pii/S092702481100050X>
- [18] Duran E, Piliouline M, Sidrach-De-Cardona M, Galan J, Andujar JM. Different methods to obtain the I-V curve of PV modules: A review. *Conf Rec IEEE Photovolt Spec Conf*. 2008;
- [19] Velilla E, Cano JB, Jaramillo F. Monitoring system to evaluate the outdoor performance of solar devices considering the power rating conditions. *Sol Energy* [Internet]. Elsevier; 2019;194:79-85. Available from: <https://doi.org/10.1016/j.solener.2019.10.051>
- [20] Velilla E, Ramirez D, Uribe J-I, Montoya JF, Jaramillo F. Outdoor performance of perovskite solar technology: Silicon comparison and competitive advantages at different irradiances. *Sol Energy Mater Sol Cells* [Internet]. Elsevier B.V.; 2019;191:15-20. Available from: <https://doi.org/10.1016/j.solmat.2018.10.018>
- [21] Velilla E, Jaramillo F, Mora-Seró I. High-throughput analysis of the ideality factor to evaluate the outdoor performance of perovskite solar minimodules. *Nat Energy* [Internet]. Springer Science and Business Media LLC; 2021;6:54-62. Available from: <http://www.nature.com/articles/s41560-020-00747-9>
- [22] Meeker W, Hong Y, Escobar L. Degradation Models and Analyses. *Encycl Stat Sci* [Internet]. Hoboken, NJ, USA: John Wiley & Sons, Inc.; 2011. p. 1-23. Available from: <http://doi.wiley.com/10.1002/0471667196.ess7148>
- [23] IEC 61853-2. Photovoltaic (PV) module performance testing and energy rating-Part 2_ Spectral responsivity, incidence angle and module operating temperature measurements. 2016.
- [24] Phinikarides A, Kindyni N, Makrides G, Georghiou GE. Review of photovoltaic degradation rate methodologies. *Renew Sustain Energy Rev*. [Internet]. Elsevier; 2014;40:143-152. Available from: <http://dx.doi.org/10.1016/j.rser.2014.07.155>
- [25] He S, Qiu L, Ono LK, Qi Y. How far are we from attaining 10-year lifetime for metal halide perovskite solar cells? *Mater Sci Eng R Reports* [Internet]. Elsevier Ltd.; 2020;140:100545. Available from: <https://linkinghub.elsevier.com/retrieve/pii/S0927024820300545>

elsevier.com/retrieve/pii/S0927796X20300036

[26] Boyd CC, Cheacharoen R, Leijtens T, McGehee MD. Understanding Degradation Mechanisms and Improving Stability of Perovskite Photovoltaics. *Chem Rev.* [Internet]. American Chemical Society; 2019;119:3418-3451. Available from: <http://pubs.acs.org/doi/10.1021/acs.chemrev.8b00336>

[27] Bisquert J, Juarez-Perez EJ. The Causes of Degradation of Perovskite Solar Cells. *J Phys Chem Lett* [Internet]. American Chemical Society; 2019;10:5889-5891. Available from: <https://pubs.acs.org/doi/10.1021/acs.jpcllett.9b00613>

[28] McLeod JA, Liu L. Prospects for Mitigating Intrinsic Organic Decomposition in Methylammonium Lead Triiodide Perovskite. *J Phys Chem Lett* [Internet]. 2018;9:2411-2417. Available from: <https://pubs.acs.org/doi/10.1021/acs.jpcllett.8b00323>

[29] Heo S, Seo G, Lee Y, Seol M, Kim SH, Yun D-J, et al. Origins of High Performance and Degradation in the Mixed Perovskite Solar Cells. *Adv Mater* [Internet]. 2019;31:1805438. Available from: <http://doi.wiley.com/10.1002/adma.201805438>

[30] Yang B, Suo J, Mosconi E, Ricciarelli D, Tress W, De Angelis F, et al. Outstanding Passivation Effect by a Mixed-Salt Interlayer with Internal Interactions in Perovskite Solar Cells. *ACS Energy Lett* [Internet]. American Chemical Society (ACS); 2020;5:3159-67. Available from: <https://pubs.acs.org/doi/10.1021/acsenerylett.0c01664>

[31] Zhang S, Liu Z, Zhang W, Jiang Z, Chen W, Chen R, et al. Barrier Designs in Perovskite Solar Cells for Long-Term Stability. *Adv Energy Mater* [Internet]. 2020;2001610:2001610. Available from: <https://onlinelibrary.wiley.com/doi/abs/10.1002/aenm.202001610>

[32] Liu Z, Qiu L, Ono LK, He S, Hu Z, Jiang M, et al. A holistic approach to interface stabilization for efficient perovskite solar modules with over 2,000-hour operational stability. *Nat Energy* [Internet]. Springer US; 2020; Available from: <http://dx.doi.org/10.1038/s41560-020-0653-2>

[33] IEC 61215-1-4. IEC 61215-1-4. Terrestrial photovoltaic (PV) modules – Design qualification and type approval – Part 1-4: Special requirements for testing of thin-film Cu(In,Ga)(S,Se)₂ based photovoltaic (PV) modules. 2016;

[34] Makrides G, Zinsser B, Norton M, E. G. Performance of Photovoltaics Under Actual Operating Conditions. *Third Gener Photovoltaics* [Internet]. InTech; 2012. Available from: www.intechopen.com

[35] Dash PK, Gupta NC, Rawat R, Pant PC. A novel climate classification criterion based on the performance of solar photovoltaic technologies. *Sol Energy* [Internet]. Elsevier Ltd.; 2017;144:392-8. Available from: <http://dx.doi.org/10.1016/j.solener.2017.01.046>

[36] Khadka DB, Shirai Y, Yanagida M, Miyano K. Degradation of encapsulated perovskite solar cells driven by deep trap states and interfacial deterioration. *J Mater Chem C* [Internet]. The Royal Society of Chemistry; 2018;6:162-170. Available from: <http://xlink.rsc.org/?DOI=C7TC03733C>

[37] Ma C, Shen D, Qing J, Thachoth Chandran H, Lo M-F, Lee C-S. Effects of Small Polar Molecules (MA + and H₂O) on Degradation Processes of Perovskite Solar Cells. *ACS Appl Mater Interfaces* [Internet]. 2017;9:14960-14966. Available from: <http://pubs.acs.org/doi/10.1021/acsam.7b01348>

[38] Lee H, Lee C, Song H-J. Influence of Electrical Traps on the Current Density Degradation of Inverted Perovskite Solar Cells. *Materials (Basel)* [Internet].

MDPI AG; 2019;12:1644. Available from: <https://www.mdpi.com/1996-1944/12/10/1644>

[39] Jain A, Kapoor A. A new method to determine the diode ideality factor of real solar cell using Lambert W-function. *Sol Energy Mater Sol Cells*. 2005;85:391-396.

[40] Kerr MJ, Cuevas A. Generalized analysis of the illumination intensity vs. open-circuit voltage of solar cells. *Sol Energy*. 2004;76:263-267.

[41] Santakrus Singh N, Jain A, Kapoor A. Determination of the solar cell junction ideality factor using special trans function theory (STFT). *Sol Energy Mater Sol Cells* [Internet]. Elsevier; 2009;93:1423-1426. Available from: <http://dx.doi.org/10.1016/j.solmat.2009.03.013>

[42] Bashahu M, Nkundabakura P. Review and tests of methods for the determination of the solar cell junction ideality factors. *Sol Energy* [Internet]. 2007;81:856-863. Available from: <https://linkinghub.elsevier.com/retrieve/pii/S0038092X06002842>

[43] Tress W, Yavari M, Domanski K, Yadav P, Niesen B, Correa Baena JP, et al. Interpretation and evolution of open-circuit voltage, recombination, ideality factor and subgap defect states during reversible light-soaking and irreversible degradation of perovskite solar cells. *Energy Environ Sci* [Internet]. Royal Society of Chemistry; 2018;11:151-65. Available from: <http://dx.doi.org/10.1039/C7EE02415K>

[44] Agarwal S, Seetharaman M, Kumawat NK, Subbiah AS, Sarkar SK, Kabra D, et al. On the Uniqueness of Ideality Factor and Voltage Exponent of Perovskite-Based Solar Cells. *J Phys Chem Lett* [Internet]. 2014;5:4115-21. Available from: <https://pubs.acs.org/doi/10.1021/jz5021636>

[45] Wetzelaer G-JAH, Scheepers M, Sempere AM, Momblona C, Ávila J, Bolink HJ. Trap-Assisted Non-Radiative Recombination in Organic-Inorganic Perovskite Solar Cells. *Adv Mater* [Internet]. 2015;27:1837-41. Available from: <http://doi.wiley.com/10.1002/adma.201405372>

[46] Marinova N, Tress W, Humphry-Baker R, Dar MI, Bojinov V, Zakeeruddin SM, et al. Light Harvesting and Charge Recombination in CH₃NH₃PbI₃ Perovskite Solar Cells Studied by Hole Transport Layer Thickness Variation. *ACS Nano* [Internet]. 2015;9:4200-9. Available from: <http://pubs.acs.org/doi/abs/10.1021/acsnano.5b00447>

[47] Almora O, Cho KT, Aghazada S, Zimmermann I, Matt GJ, Brabec CJ, et al. Discerning recombination mechanisms and ideality factors through impedance analysis of high-efficiency perovskite solar cells. *Nano Energy* [Internet]. Elsevier Ltd.; 2018;48:63-72. Available from: <https://doi.org/10.1016/j.nanoen.2018.03.042>

[48] Contreras-Bernal L, Ramos-Terrón S, Riquelme A, Boix PP, Idígoras J, Mora-Seró I, et al. Impedance analysis of perovskite solar cells: A case study. *J Mater Chem A* [Internet]. Royal Society of Chemistry; 2019;7:12191-200. Available from: <http://xlink.rsc.org/?DOI=C9TA02808K>

[49] Velilla E, Cano J, Jimenez K, Valencia J, Ramirez D, Jaramillo F. Numerical Analysis to Determine Reliable One-Diode Model Parameters for Perovskite Solar Cells. *Energies* [Internet]. 2018;11:1963. Available from: www.mdpi.com/journal/energies

[50] Cotfas DT, Cotfas PA, Kaplanis S. Methods to determine the dc parameters of solar cells: A critical review. *Renew Sustain Energy Rev*. [Internet]. Elsevier; 2013;28:588-596. Available from: <http://dx.doi.org/10.1016/j.rser.2013.08.017>

[51] Guerrero A, You J, Aranda C, Kang YS, Garcia-Belmonte G, Zhou H, et al. Interfacial Degradation of Planar Lead Halide Perovskite Solar Cells. *ACS Nano* [Internet]. 2016;10:218-224. Available from: <https://pubs.acs.org/doi/10.1021/acsnano.5b03687>

IntechOpen

IntechOpen